Magnetic properties and interaction mechanisms of iron-based core–shell structures prepared by sputtering at low substrate temperatures

2008 J. Phys.: Condens. Matter 20 085216

(http://iopscience.iop.org/0953-8984/20/8/085216)

IOP PUBLISHING JOURNAL OF PHYSICS: CONDENSED MATTER

J. Phys.: Condens. Matter **20** (2008) 085216 (10pp) doi:10.1088/0953-8984/20/8/085216

Magnetic properties and interaction mechanisms of iron-based core–shell structures prepared by sputtering at low substrate temperatures

F Jiménez-Villacorta and C Prieto

Instituto de Ciencia de Materiales de Madrid, Consejo Superior de Investigaciones Científicas, Cantoblanco, 28049-Madrid, Spain

Received 19 November 2007, in final form 14 January 2008
Published 1 February 2008
Online at stacks.iop.org/JPhysCM/20/085216

Abstract

The magnetic properties of partially oxidized nanocrystalline iron thin films prepared by DC-magnetron sputtering at low substrate temperatures in the 175–300 K range are studied. The preparation method is presented as a simple method for fabricating granular structures. Films prepared at intermediate temperatures exhibit granular magnetic behaviour, in which nanocrystalline grains act as almost decoupled particles, surrounded by an oxide shell, forming exchange bias core–shell systems. The magnetic features of granular systems obtained by this new method are described and the mechanisms of interaction between metallic grains and their oxide shells are explained, as are their effects in the magnetization reversal process.

1. Introduction

Granular systems exhibiting core–shell morphology present a considerable interest not only for potential technological applications but also from a purely scientific point of view. A wide range of striking phenomena can be attributed to reduced size and surface effects and also to interactions between particles with their own shell and between particles themselves across their respective shells. For instance, structural disorder in the surface of magnetic particles have been always considered to play a decisive role in some magnetic nanoscopic features, such as spin-glass-like behaviour of the surface spins [1, 2]. By merely considering the interparticle interactions in a granular system, it has been reported that different combinations of anisotropy, exchange and dipolar interactions can modify the blocking temperature, either increasing [3] or decreasing [4] the energy barriers with rising interactions, even leading in the last case to interpretations based on collective ordering that induces a collective magnetic behaviour from a distribution of individual superparamagnetic moments [5–7]. Also, magnetic features ascribed to exchange interactions between the core and shell (or interface) spins are determined by the constituent species forming both core and shell phases. Hence, well controlled modulation of the structural and compositional features of such granular materials can lead not only to the development of new materials with outstanding properties, but also to a better understanding of the involved physical phenomena.

Heterogeneous two phase magnetic structures, consisting on a transition metal (TM) and its correspondent oxide (TMO) have been largely investigated as magnetic granular systems formed by ferromagnetic particles in an antiferromagnetic matrix [8], core–shell systems [9, 10] and thin films [11]. TM/TMO systems present a very fascinating effect attributed to spin interactions between the metal and the oxide, resulting in an overcome of the superparamagnetic effect, enhancement of coercivity and, if the oxide component has sufficiently large anisotropy, exchange bias [12, 13]. Moreover, exchange bias has been proposed as an appropriate mechanism to stabilize magnetization in nanostructures against thermal fluctuations [8]. Although the low blocking temperatures observed for TM/TMO systems might limit their potential applications (for instance in Fe/FeO systems, the exchange bias effect disappears at $T \approx 50$ K) [14], nanoparticles with modified surface have become good candidates for magnetic decoupling, and possible applications in magnetic recording [12, 15].

In this work, we report on the magnetic properties of the core–shell system that can be prepared by sputtering deposition of iron thin films onto substrates at low temperatures and then

oxidizing in a controlled way [16]. Moreover, we show that this is a simple and alternative method to fabricate nanostructured TM/TMO systems presenting the above commented magnetic granular features. It should be pointed out that films prepared at temperatures far lower than the room temperature behave as almost decoupled grains in a particle system [17]. The magnetic study of the films is thoroughly developed based on magnetothermal analysis provided by zero field cooling–field cooling (ZFC–FC) magnetization curves, thermoremanent magnetization curves and magnetization loops at different temperatures. Furthermore these magnetic properties are correlated with the previously reported microstructural and compositional features [16] and transport properties [17]. Finally, an attempt to elucidate the interaction mechanisms between the metallic grains forming the ferromagnetic phase and the oxide surrounding them has been developed in order to model the exchange bias phenomenology at low temperatures in these core/shell systems.

2. Experimental details

Iron thin films, with 100 nm nominal thickness, were grown by sputtering on naturally oxidized Si(100) substrates using a DC-operated 2 inch planar magnetron source (from Angstrom Sciences). Base pressure was in the high vacuum range (10^{-7} mbar) and Ar pressure during the sputtering process was 5.0×10^{-3} mbar. Deposition rate of 1.2 nm min^{-1} was obtained after applying a power to the magnetron less than 10 W. The experimental set-up has the possibility of keeping the substrate temperature constant during deposition, by using a home-modified Oxford Instrument CF-100 continuous flow cryostat placed inside the vacuum chamber. An ITC-502 temperature controller allows setting the substrate temperature with a precision better than 1 K. Moreover, in order to deposit a cap layer, there exists the possibility of changing sputtering targets maintaining the sample in the high vacuum pressure chamber [18].

For this work, several sets of samples were deposited at different substrate temperatures, varying from 300 to 170 K. After deposition, films were oxidized '*in situ*' at room temperature by flowing oxygen at a pressure of 5×10^{-1} mbar for 1 h, and later capped with a gold layer in order to prevent from further oxidations. Reference [16] gives details of oxide types as well as the obtained amount in the samples.

Magnetic measurements were carried out in a SQUID magnetometer (MPMS-5, from Quantum Design). ZFC–FC magnetization curves were obtained at several applied constant fields, from $H = 50$ to 5000 Oe. The possible influence of the heating rate was carefully investigated in order to conclude that, within the used rates range, obtained results are independent on it. Data were collected from 5 to 350 K during heating samples with a rate of 3 K min^{-1}. Thermoremanence curves have been performed for samples prepared at 200 K at moderate (700 Oe) and high saturating fields (25 kOe), with a heating rate of 2 K min^{-1}. Magnetization loops were achieved at different temperatures, from 5 K to room temperature, under two different sequences: FC loops were performed after cooling the samples under an applied field of 20 kOe and ZFC loops after cooling samples without any applied field.

3. Results

Figure 1 depicts high-resolution transmission electron micrographs of the granular film. From such micrographs, can be estimated the grain-size distribution both 'in-plane' and 'out-of-plane' directions. Size distribution should be considered in magnetic particle systems because it will impinge directly on the magnetic properties as for example on the distribution of blocking temperatures. In figures 1(c) and (d) can be observed the narrow film grain-size distribution. Both distributions have been fitted by log-normal functions, with a standard deviation of around $\sigma \approx 0.3$. The observed differences between the average in-plane and out-of-plane grain sizes ($\langle D_{\mathrm{oop}} \rangle = 7.4$ nm and $\langle D_{\mathrm{ip}} \rangle = 5.3$ nm) are in agreement with previous x-ray diffraction characterization [18].

Figure 2 shows the magnetization loops at different temperatures of samples prepared at $T_{\mathrm{S}} = 300$ and 200 K. Measurements have been performed after cooling samples under an applied magnetic field of 20 kOe. For comparison purposes, magnetic moments are given in Bohr magnetons per Fe atom, the number of Fe atoms was estimated after ion beam analysis [19], where Rutherford and non-Rutherford experiments have been focused to obtain a precise atomic depth distribution and its corresponding atomic areal-density. Loops show usual features of ferromagnetic polycrystalline thin films, with small variation with temperature of magnetization values. Otherwise, samples prepared at $T_{\mathrm{S}} = 200$ K present exchange bias [20] for loops measured at low temperatures and disappears over 20 K. This anisotropy stems from the exchange interactions between the spins of ferromagnetic iron grains and those from the antiferromagnetic (or magnetically frozen) oxide phase. This feature is not observed in films prepared at temperatures different from 200 K, showing that the pinning exerted by the oxide phase spins seems to be not such effective. The exchange anisotropy for low temperature films results in an enhanced remanence and coercivity at low temperatures, thus leading to a more square shape of the loops than for the films prepared at higher temperatures. Well over 50 K (when exchange anisotropy is absent) this squareness disappears and loops shape are almost similar for all samples.

ZFC–FC measurements of samples prepared at $T_{\mathrm{S}} = 250$ and 200 K are shown in figure 3, for different applied constant fields in the 50–5000 Oe range. All the films present ferromagnetic character, even well above the room temperature. The FC magnetization behaviour shows a weak dependence with temperature, as it is usually observed in interacting particle systems [21]. For samples prepared at high temperature (figure 3(a)), a monotonic and smooth temperature dependence is observed at the ZFC curves below the irreversibility temperature (T_{irr}, merging point between ZFC and FC curves), also in agreement with highly interacting ferromagnetic systems [22]. It is worth to point out briefly, that a slight increase with temperature of the FC magnetization is observed below T_{irr}. This behaviour could be explained in two different ways: it could be ascribed to strong interactions

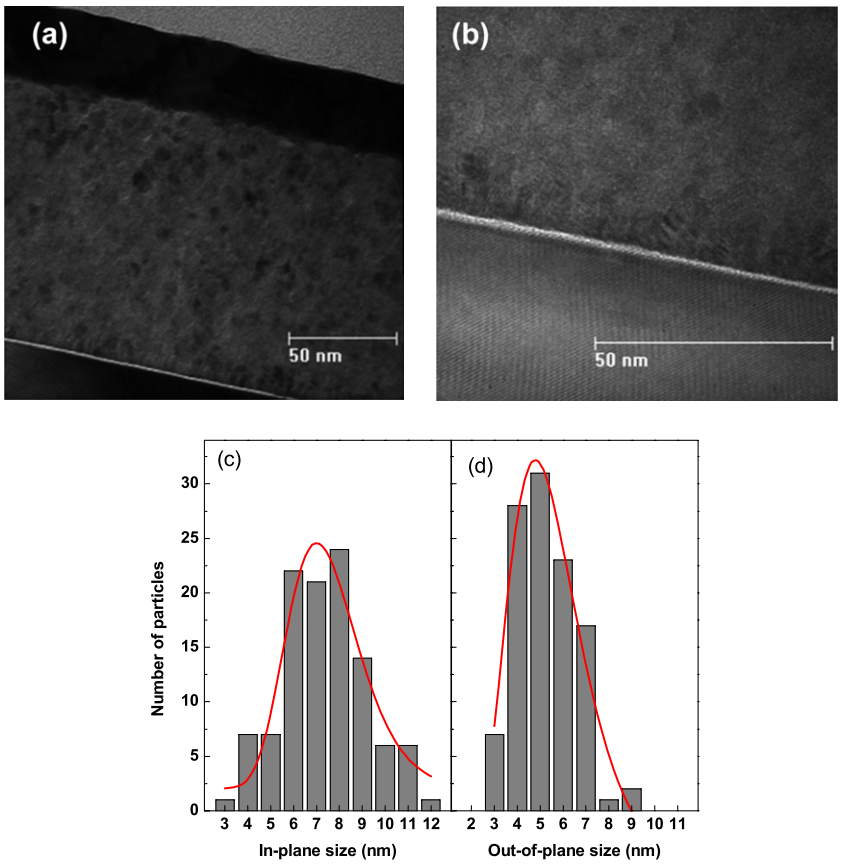

Figure 1. (a), (b) High-resolution micrographs of the $T_S = 200$ K film. (c) Distribution of the in-plane grain-size dimensions. (d) Distribution of the out-of-plane grain-size dimensions.

(This figure is in colour only in the electronic version)

between grains, both dipolar force and exchange coupling between neighbour grains, or to temperature dependence of the anisotropy constant [22, 23]. For these samples, the first explanation seems to be reasonable, since specimens prepared at high temperatures (figure 3(a)), are poorly oxidized and hence they should present high packing density of grains with dipolar and exchange coupling existing between neighbour grains in a more remarkable manner. In contrast, for films prepared at $T_S = 200$ K, the ZFC curves below T_{irr} (figure 3(b)) show a strong temperature dependence on magnetization, being similar to the usual blocking behaviour in a particle system. This agrees with the intergranular tunnelling phenomena observed in the low temperature films by magnetotransport analysis.

Temperature dependence of the difference between ZFC and FC magnetization curves (M_{FC}–M_{ZFC}) provides similar information as the low-field thermo-remanence magnetization (TRM) curves. TRM magnetization at these fields represents the irreversible contribution of the particles blocked in the direction of the field. It must be taken into account as well that the low-field measurements probe a collective response of the particles with only weak relative reorientation between the particle moments. Figure 4(a) shows the comparison between the TRM curve obtained for $T_S = 200$ K sample measured after cooling with an applied field of 700 Oe and the corresponding (M_{FC}–M_{ZFC}) measured at 700 Oe.

Figure 4(b) shows the TRM curve of a $T_S = 200$ K sample measured after cooling with 25 kOe. The temperature dependence of the TRM curve matches quite well with the values of remanence obtained in the hysteresis loops. The study of this temperature decay of magnetization is found to be very useful in the study of the energy considerations of particle systems. Results obtained from the analysis of this curve will be discussed in section 4.3.

4. Discussion

4.1. Hysteresis loops

The evolution of remanence (figure 5(a)) shows important differences between the film prepared at $T_S = 200$ K and the rest. That sample reflects an important decay of the remanence values with increasing temperature, unlike the rest of the films, which present a hardly smooth decrease. Inset of figure 5(a) shows the evolution of magnetization values at $T = 10$ K for the film series. A reduction in the magnetization is observed with decreasing T_S, presenting a minimum for $T_S = 200$ K. The magnetic moment evolves from $\sim 2\ \mu_B$ per Fe atom (near the iron bulk value of 2.2 μ_B/at) for the film prepared at room temperature, to 1.08 μ_B per atom in the $T_S = 200$ K sample. After estimation, taking into account the magnetic moments of iron present in metallic and oxide

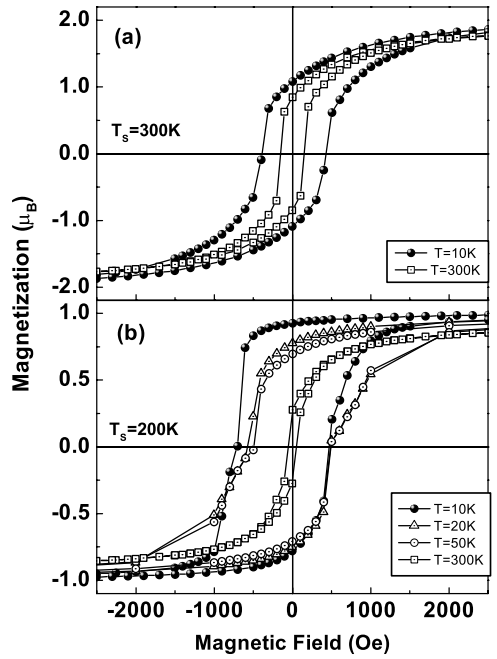

Figure 2. FC magnetization loops at different temperatures of samples prepared at (a) $T_S = 300$ K; (b) $T_S = 200$ K.

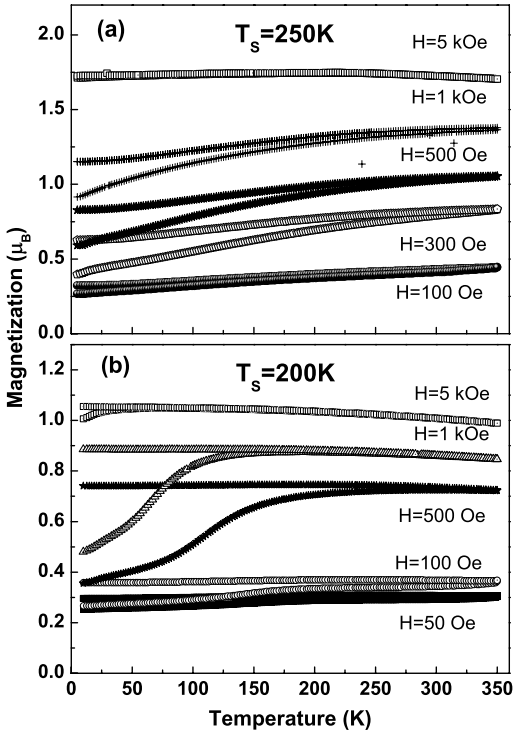

Figure 3. FC-ZFC magnetization curves for different applied fields. (a) $T_S = 250$ K sample; (b) $T_S = 200$ K sample.

phases, it can be concluded that this diminution is mainly due to an increasing presence of oxide phases. A decrease in the growth temperature implies a reduction in the average grain dimensions that leads to an enhancement of the surface to volume ratio, resulting in a higher degree of oxidation [18]. Thus, little effect from spin canting or magnetically dead

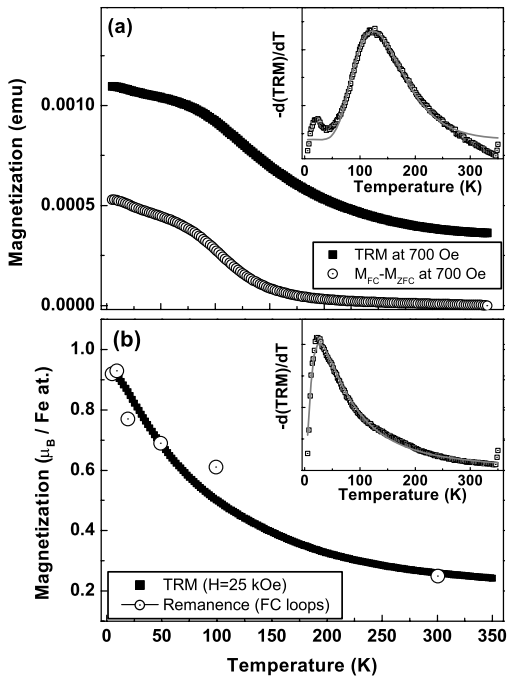

Figure 4. (a) Thermo-remanence magnetization curves of the $T_S = 200$ K film at low fields ($H = 700$ Oe), and M_{FC}–M_{ZFC} curve for the same film, for comparison; (inset: temperature derivatives of the TRM curve fitted by a log-normal function). (b) Thermo-remanence magnetization at saturating fields ($H = 25$ kOe) of the sample prepared at $T_S = 200$ K; (inset: temperature derivatives of the TRM curve fitted by a log-normal function).

layers [24, 25] at the grain surfaces can be deduced, which is in agreement with the exchange interaction between spins at the metallic grain surface with spins at the oxide phase. However, the magnetization value for the sample prepared at $T_S = 170$ K is slightly higher than that for the $T_S = 200$ K specimen. Since the previous compositional characterization asserts that this sample presents a higher degree of oxidation respect to the rest of the films, it should be concluded that this higher oxidation leads to the formation of a higher amount of ferrimagnetic species contributing to the total magnetization, such as Fe_3O_4 and γ-Fe_2O_3 [16]. This last term is in agreement with the absence of exchange anisotropy, its remanence evolution with temperature and the important increase of resistivity observed in films prepared at $T_S = 170$ K respect to the others.

Films prepared at temperatures near RT and at $T_S = 170$ K present a slow decrease in coercivity with increasing temperature, as expected for ferromagnetic thin films with ferromagnetic ordering temperatures quite higher than the measurement range temperatures. However, the temperature evolution of FC loops obtained for specimen prepared at $T_S = 200$ K reveal interesting results. The coercivity has a steeper decrease with increasing temperature. Figure 5(b) shows that the coercive field follows rather well the expression:

$$H_C(T) = H_C(0)\left[1 - (T/T_0)^{0.77}\right] \quad (1)$$

(with $T_0 \approx 360$ K) proposed for particle systems with randomly oriented anisotropy axes [26], in agreement with the

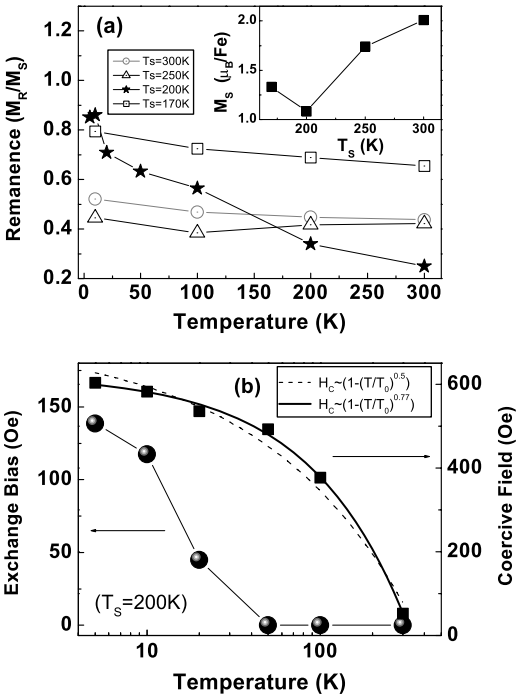

Figure 5. (a) Evolution of remanence with temperature for representative films (inset: magnetization values at $T = 10$ K versus substrate preparation temperature); (b) evolution of coercivity and exchange bias versus temperature of the $T_S = 200$ K deposited film.

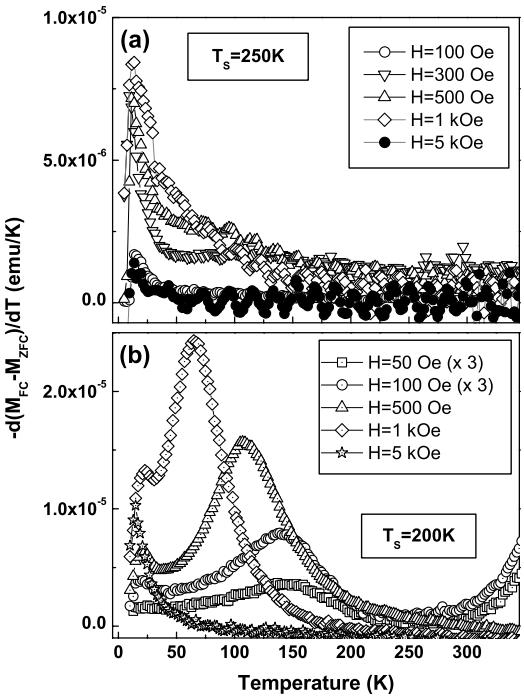

Figure 6. Temperature derivative of the zero field cooled magnetization, $\mathrm{d}(M_{\mathrm{ZFC}})/\mathrm{d}T$. (a) Sample prepared at T_S =250 K and (b) sample prepared at $T_S = 200$ K.

polycrystallinity of the sample. This evolution is similar to the classical dependence

$$H_C(T) = H_C(0)\left[1 - (T/T_0)^{1/2}\right] \tag{2}$$

for single-domain particles with easy axes aligned in the direction of the film [27], which provides a slightly worst fitting. It should be noted that the observed evolution does not seem to be remarkably altered by the existence of exchange anisotropy at low temperatures.

Thus, in principle, the samples prepared at $T_S = 200$ K presents a behaviour similar to a system of non-interacting (or weakly interacting) particles. The oxide phase at temperatures higher than its blocking temperature provides, in some manner, a decoupling effect of iron nanograins and coercivity can be described as an intragrain phenomenon.

4.2. ZFC–FC magnetization curves

In a particle system, ZFC magnetization curves represent the total amount of magnetic moments that have been polarized in the direction of the measuring applied field. As the temperature increases, the bigger particles, which were in a blocked state, begin to orientate along the field, overcoming the energy barrier by thermal effects [28]. Jumps observed in the ZFC curves corresponding to $T_S = 200$ K samples are similar to an 'activation energy' and suggest that the spin system evolve from a random spin state to a highly spin state polarized in the direction of the applied field. Thus, these samples follow the usual blocking behaviour of particle systems and also are in agreement with the intergranular tunnelling phenomena observed by magnetotransport analysis.

ZFC–FC information is complementary of the obtained from hysteresis loops data. As it is deduced from figure 3, the effect of increasing the applied field is to decrease the energy barrier, that is, the average blocking temperature. On this way, the analysis of the M_{FC}–M_{ZFC} derivatives (as well as the ZFC magnetization curve derivatives) has been used to evaluate qualitatively the distribution of blocking temperatures (T_B) in particle systems [5, 29]. Furthermore, since $T_B \sim KV$ (being K the anisotropy constant and V the particle volume), the T_B distribution can be directly associated to the particle size distribution particle sizes. In the inset of figure 4(a) it is shown that the distribution of energy barriers can be fitted by a grain-size log-normal distribution:

$$f(d) = \frac{1}{\sqrt{2\pi}\sigma_d d}\exp\left(\frac{\ln^2(d/d_0)}{2\sigma_d^2}\right) \tag{3}$$

where d are grain-size diameters, d_0 is the average diameter and σ_d is the standard deviation.

The temperature dependence of magnetic evolution in films prepared at $T_S = 250$ and 200 K are illustrated by their respective temperature derivative curves $[\mathrm{d}(M_{\mathrm{ZFC}})/\mathrm{d}T]$ in figure 6. The $T_S = 200$ K sample presents an interesting feature: two peaks appear in the measured range. The first one (hereafter, T_1), remains almost constant at 20 K independently of the applied field. The second one (T_2) shifts to low temperatures and becomes narrow as the applied field increases. That contrasts with the monotonic behaviour of the sample fabricated at $T_S = 250$ K, in which it is

observed, however, an small peak in the derivative curves $[d(M_{FC}-M_{ZFC})/dT]$ fixed around 20 K.

T_1 stems from a subtle increase in the ZFC magnetization (as can be observed in figure 3(b)) and is associated to the onset of a deblocking process. Here, the frozen spins from the oxide phase begin to thermally polarize, orientating in the direction of the applied field and, in part, begin to contribute to the total magnetization by means of their ferrimagnetic species. At this temperatures range, the change in magnetic state has also its effect in the interaction with the ferromagnetic core spins, resulting in the previously observed extinction of exchange anisotropy in the FC magnetization loops.

The main feature of the $(M_{FC}-M_{ZFC})$ temperature derivative curves is a field dependent peak that is associated to the blocking temperature distribution of the magnetic particle system. The temperature of such peak maximum (T_2) represents the steeper variation of the ZFC branch and it can be established that T_2 corresponds to the average value of blocking temperature distribution.

It is well known that, for a fine particle system, the increase of the applied magnetic field will reduce the height of the energy barrier for spin rotation and hence a decrease in the associated blocking temperature [30]. From the classical theory of Néel [31], the field dependence of the blocking temperature follows the expression:

$$\Delta E = k_B T_B(H) = KV(1 - H/H_K)^2 \tag{4}$$

where k_B is the Boltzman constant, K is the anisotropy constant and H_K is the anisotropy field. On the other hand, interacting particle systems have been reported to show a $(1 - H/H_K)^{2/3}$ spin-glass-like behaviour [32, 33], analogue to canonical spin glass systems [34]. Nevertheless, Wenger and Mydosh [35] have concluded that the whole dependence is $T_B \sim (1 - H/H_K)^2$ for small fields and $T_B \sim (1 - H/H_K)^{2/3}$ for large fields. Finally, Victora proposed a blocking temperature evolution of a single-domain particle assembly [36] that has been checked experimentally [5] with the expression:

$$T_B = \frac{KV}{k_B \ln(\tau_m/\tau_0)}\left[1 - \frac{H}{H_K}\right]^{3/2} \tag{5}$$

where τ_m is the observation time and τ_0 is a characteristic time (typically $\tau_0 \sim 10^{-9}$ s). Figure 7(a) depictures the obtained dependence of T_2 for films prepared at $T_S = 200$ K showing rather well a $T_B \sim (1 - H/H_K)^{3/2}$ dependence for intermediate fields, which is another evidence that those samples actually consist on a magnetic particle system.

From the merging point where the ZFC and FC branches coincide, we extract the irreversibility temperature values, T_{irr}, defined as the highest blocking temperature. In our measurements, this merging point is selected as the temperature value where the difference between the field cooled and the zero field cooled data is less than 2% the FC value:

$$\Delta M(T_{irr}) = \frac{M_{FC} - M_{ZFC}}{M_{FC}} \leqslant 0.02.$$

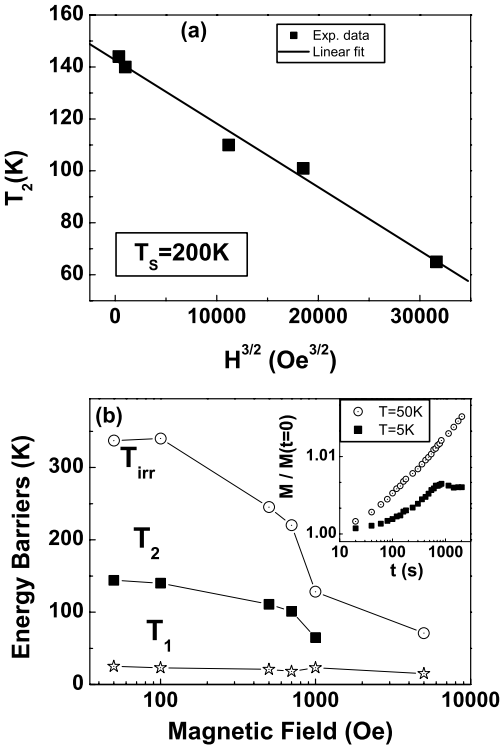

Figure 7. (a) Field dependence of the T_2 peak, associated to the mean blocking temperature for the granular sample; (b) evolution of energy barriers, T_1, T_2 and irreversibility temperature respect to the applied field, and its magnetization, $M(T_{irr})$; (inset: magnetization versus time of a $T_S = 200$ K sample, for a constant field of $H = 700$ Oe and for $T = 5$ and 50 K).

In figure 7(b), the evolution of the energy barriers T_1, T_2 and T_{irr} with the applied field is represented. There seems to exist a correlation between the irreversibility temperature and this T_2 peak. The irreversibility temperature is directly related to the mean blocking temperature, since T_{irr} can be considered as an analogous term to the glass temperature (T_G) or maximum temperature (T^{max}) [4], studied in fine particle systems and defined as the cusp or the maximum value of the ZFC curve. However, our ZFC magnetization curves does not have a clear maximum as in FM systems, since they present a very weak dependence on temperature above T_{irr}. For a distribution of particle sizes a shift has been observed in the maximum of ZFC magnetization to a temperature $T^{max} = \beta\langle T_B\rangle$, where β is of the order of ~2 [37, 38]. In our case, by considering the T_{irr} value as an analogous of T^{max} for particle systems, it is obtained a ratio of ~2.2 between T_{irr} and T_2. At low fields ($T \leqslant 100$ Oe) the irreversibility values decrease slightly with increasing field. This effect has been observed in randomly oriented particle systems, in which the field reduces the energy barriers of particles in a different way, depending on the orientation of their easy axes, even showing a broadening of the energy distribution [39].

Now, we focus our attention in the lowest temperatures around the energy barrier T_1, present in all the oxidized samples. The inset of figure 7(b) shows the magnetization evolution of the granular film with time at temperatures below and over T_1, with an intermediate field applied of 700 Oe. At

temperatures below T_1 ($T = 5$ K curve) the magnetization hardly increases. In fact, at $T > 500$ s, M remains practically constant and does not increase any more. On the other hand, at temperatures above T_1 (such as $T = 50$ K), the system presents a slight but continuous increase of the magnetization due to thermal activation. Hence, the scenario can be depicted as follows: at low temperatures and at low and intermediate fields, the sample prepared at $T_S = 200$ K behaves like a randomly oriented particle system; at temperatures below T_1, the sample behaves like a frozen system, similar to a spin glass; when temperature rises across T_1, the oxide phase unfreezes and the specimen slowly begins to evolve to a thermally activated state. Thus, T_1 represents a switching energy in the phenomenon of reorientation of the oxide phase spins. This results in an abrupt, but small increase of the magnetization (respect to the continuous increase of the magnetization). The continuous increase of magnetization of the ZFC curves at intermediate fields from the lowest temperatures, going through T_2, and ending in the irreversibility region, comes mainly from the thermal alignment of the particle spins towards the direction of the applied field, according to their distribution of particle sizes.

4.3. Anisotropy constant

The TRM measured at saturating fields (magnetization decay of remanence), showed in figure 4(b) for the $T_S = 200$ K film, differs from other kinds of measurements since it starts from a state where all the moments are nearly aligned along the strong applied field. Thus, the difference in both distributions obtained from low and high field measurement of the TRM is due to the fact that measurements at low applied fields are greatly affected by particle interactions while those made at high fields are particles behaviour independent [5, 28]. By definition, the remanence curve at high saturating fields can be expressed as [29]:

$$TRM\,(T) \propto \int_{T/\langle T_B\rangle}^{\infty} f\,(T_R)\,\mathrm{d}T_R \qquad (6)$$

where $T_R = T_B/\langle T_B\rangle$ are the reduced blocking temperatures, $f(T_R)$ is the blocking temperature distribution and $\langle T_B\rangle$ is the mean blocking temperature. Thus the derivative of the remanence curve (shown in the inset of figure 4(b)) gives a measurement of the blocking temperature distribution. Since the blocking temperature is directly related to the size of the particles, the blocking temperature distribution should have the same shape of grain-size distribution [33]. By fitting the derivative curve to the log-normal distribution, an average value of $\langle T_B\rangle = 76$ K is obtained for that distribution. Both, the distribution of blocking temperatures and the distribution of sizes readily fit to log-normal functions and, as a first approach, they are linked by the Néel–Arrhenius expression for thermal activation reversal in a magnetic particle system:

$$KV = k_B T_B \ln\left(\tau_m/\tau_0\right). \qquad (7)$$

Taking an observation time of $\tau_m \sim 60$ s, a characteristic time of $\tau_0 \sim 10^{-9}$ s and the mean value of the blocking temperature, this leads to an estimation of the anisotropy value of $K = 3.2 \times 10^6$ erg cm^{-3}. This result matches quite well with the estimation of the anisotropy from the $\sim(1 - H/H_K)^{3/2}$ dependence of the average blocking temperatures observed previously for intermediate fields (equation (4) gives $K = 4 \times 10^6$ erg cm^{-3}). This enhanced anisotropy respect to the bulk Fe value ($K = 4.8 \times 10^5$ erg cm^{-3}), by an order of magnitude, may be attributed to both typical increase of anisotropy observed in nanostructured systems [40, 41] and exchange bias effects due to interaction mechanisms between the spins from the oxide phase and the core FM spins.

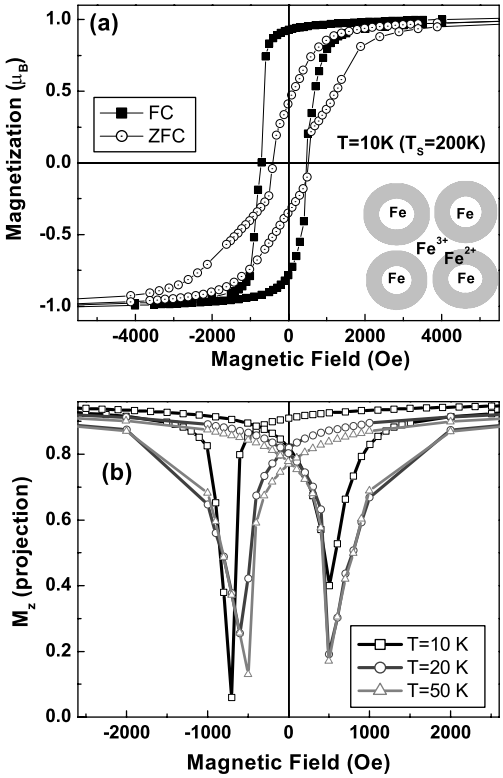

Figure 8. (a) Magnetization loops at $T = 10$ K, with (FC loop) and without (ZFC loop) an applied field during cooling, of the $T_S = 200$ K films; (inset: schematic picture of the core–shell iron–iron oxide system from the structural, compositional and magnetic study of the granular films prepared at $T_S = 200$ K). (b) Normalized magnetization projection along the field axis in the whole loop measurements at these temperature.

4.4. Interaction mechanism

Finally, we focus our attention in the interaction mechanisms between the spins from the FM iron grains and those from the oxide phase. In figure 8(a), two isotherm loops at $T = 10$ K for the $T_S = 200$ K film are displayed. One of them was obtained after cooling sample under an applied field of $H = 20$ kOe. The other was obtained by previously cooling without any field applied. It is useful to point out first the absence of exchange bias in the ZFC loop, because exchange anisotropy only appears when the temperature decreases across the blocking temperature of the antiferromagnetic oxide under applied field. Moreover, the FC loop presents a quite high remanence being

very similar to the saturation magnetization ($\approx 0.94 M_S$) due to magnetic stabilization brought about by exchange anisotropy; conversely in the ZFC loop, the remanence value becomes considerably reduced ($\approx 0.43 M_S$) being near one half of the saturation value. This result is in very good agreement within the framework of the Stoner–Wohlfarth model for randomly oriented non-interacting fine particles [42].

Regarding the exchange anisotropy, a necessary condition to observe exchange bias in FM/AFM bilayer systems is to fulfil the following condition [13]: $K_{AFM} t_{AFM} \geqslant J_{int}$, where K_{AFM} is the anisotropy of the AFM layer, t_{AFM} its thickness and J_{int} the exchange constant in the FM/AFM interface. Since the exchange constant is related to the exchange field by equation $H_e = J_{int}/M_{FM} t_{FM}$, it is possible to estimate the exchange constant. Assuming an oxide shell of 2 nm, estimated from combined Rutherford backscattering spectroscopy and transmission electron microscopy analysis [16] (that provides $t_{AFM} \approx 4$ nm as average thickness for the AFM oxide) and an average FM core size of $t_{FM} \approx 6$ nm, and taking into account the bulk value for the grain magnetization ($M_{FM} \approx 1730$ emu cm^{-3}) it is possible to estimate the exchange constant at $T = 10$ K as $J_{int} \approx 0.24$ erg cm^{-3}, and finally to obtain a minimum value for the anisotropy as $K_{AFM} \geqslant 1.3 \times 10^6$ erg cm^{-3}.

Characterization techniques have provided useful information of the insight microstructure of films showing granular behaviour. For instance, it has been deduced that an important amount of Fe^{2+} is present in the oxide phase [16] that corresponds undoubtedly to the antiferromagnetic FeO and the ferrimagnetic Fe_3O_4. Giving a model to explain the oxidation process of nanograins, it seems reasonable that this purely ferrous FeO phase would be placed at the core–shell interface, between the pure metallic Fe and the oxide region, whereas the ferric species would be present between the Fe–FeO core–shell structures in a configuration similar to the depicted in the inset of figure 8(a).

The challenge in interpreting the exchange bias mechanism in FM/AFM core–shell nanostructures resides in the presence of spin frustration and uncompensated interfacial spins, in contrast to simple models for perfect-layered systems. This will impinge on, for example, the effective pinning of the AFM phase through the direction parallel to the applied magnetic field. To understand qualitatively the interactions between the metallic core and the oxide shell it can be useful to evaluate the projection of the magnetization along the applied field direction, $M_z \propto |M \cdot H|$ or $M_z \propto |M \cdot \cos\theta|$, where θ is the angle between the virtual total reversal magnetization and the field axis [43].

In figure 8(b), that projection is illustrated for the loops of figure 2(b) obtained at 10, 20 and 50 K. Assuming that the net magnetization comes mainly from the metallic core spins, we observe different evolutions of the magnetization projections through the reversal processes in the descending and ascending branches for the measurements taken at 10 K. The peak corresponding to the coercive field range in the descending branch is narrower and symmetric. A stronger exchange coupling at the interface (as it occurs at $T = 10$ K) results in a faster reversal of spins ferromagnetically aligned with the antiferromagnetic shell [44]. This sharp evolution seems to indicate a reversal process by almost uniform rotation of the particle spins. In contrast, the ascending branch presents an asymmetric and wider peak, which can be interpreted in terms of domain formation beginning at the interface, and a subsequent propagation through the inner regions of the core. An analogous phenomenology has also been observed in FM/AFM bilayers when the cooling field is applied in directions not aligned to the anisotropy axis of the AFM [45], and when the cooling field is applied in easy and hard axis directions [46].

The narrow peak in the descending branch becomes broader when increasing temperature, as it can be observed at $T = 20$ and 50 K. It is important to remark first the subtle differences between the magnetization loops in these two measurement temperatures, which characterize perfectly the progressive extinction of exchange bias. As we can observe, these little differences only restrict to the field ranges between the remanence and the coercivity (the upper part of the descending branch). The rest of the magnetization loop is practically identical. The effect of the interaction between the core spins and the antiferromagnetic shell results in a smooth increase of both remanence and negative coercive values. Attending to the magnetization projection, it can be observed that increasing temperature leads to a broadening of the descending branch peak (apart from the shifting in the centre due to reducing coercivity). At 50 K, when the AFM shell becomes practically paramagnetic, the shape of the peak corresponding to the descending branch is practically identical to that of the ascending branch meaning, that when temperature increases, the reversal process turns from a quasi-uniform rotation of spins to a domain formation mode.

As a summary, the change in the reversal process can be interpreted as follows: for the lowest temperatures, the effect of the pinning state is rather effective; from the classical spin configuration applied to exchange bias systems [12, 13], spins from the FM and the AFM at the interface are parallel in the saturated state, oriented with the applied field. AFM phase spins remain blocked and the exchange energy applied to the core spins becomes important, leading to all spins from the FM phase to reverse following a rotational process when net magnetization moves away from this energetically favourable alignment. Thus, magnetization reversal occurs by rotation. Otherwise, return from negative saturation to the reorientation to the applied cooling field takes place by domain nucleation beginning at the interface. For the loops at higher temperatures, weaker values of the local exchange fields for the core spins near the interface as the temperature increases lead to the formation of domains. The oxide shell spins begin to flip, leaving to interface spins at the core to form uncompensated spins regions to conform the seeds for the formation of domains at the interface, due to inhomogeneous local exchange values between the surface spins and the inner spins. That dissimilar core pinning between the inner and the surface provides nucleation of domains at intermediate fields in the range of the coercive values.

5. Conclusions

In this work, we have investigated the magnetic properties of partially oxidized iron thin films prepared at different substrate temperatures during deposition. A simple method to fabricate systems with granular magnetic behaviour has been developed just by depositing iron thin films by sputtering at low temperatures. Films prepared at $T_S = 200$ K present an evolution of the coercivity identical to a particle system with random anisotropy axes. Also, from the ZFC–FC magnetization curves, it can be deduced that films prepared at low temperature consist essentially in granular core–shell magnetic systems, formed by ferromagnetic metallic iron grains surrounded by an iron oxide phase. At lower temperatures, magnetization loops show that spins from the iron oxide shell (mainly consisting in FeO and Fe_3O_4) behave as a spin frozen system able to interact with the ferromagnetic core spins, leading to exchange anisotropy. Over 20 K, hysteresis and magnetization curves depict an evolution of the oxide phase magnetic behaviour. From the M versus T measurements, it can be deduced that oxide phase spins evolve from that frozen configuration: spins from ferric species begin to thermally polarized and to orientate in the direction of the applied field and ferrous species spins, which are deduced to be placed at the core–shell interface, do not longer exert an effective pinning to their neighbour core Fe spins and exchange anisotropy disappears.

The relatively low blocking temperatures of the AFM phase in Fe/FeO_x system allow a detailed analysis of interactions between the ferromagnetic core and the oxide shell. This situation is excellent to study proximity effects between the two phases and to shed light to reversal mechanism for polycrystalline exchange bias core–shell systems and its dependence with temperature. Results show asymmetry in the magnetization loops at very low temperatures. Since exchange interaction between the FM and the AFM spins at the interface is sufficiently strong, the reversal mechanism from the easy parallel orientation overcoming the exchange interaction between FM and AFM spins at the interface to the antiparallel configuration (the descending branch of the magnetization loops) seems to indicate a process of uniform rotation of the FM spins. However, the ascending branch reveals a reversal mechanism governed by domain formation when the FM spins return form the negative saturation to the above mentioned parallel configuration between FM and AFM spins at the interface. The variation of the interface exchange coupling with increasing temperature, due to a progressive unfreeze of the AFM spins leads to modifications in the mechanisms of the magnetization reversal. For higher temperatures, approaching to the AFM blocking temperature, the uniform rotation mode in the descending branch turns into a slower non-uniform reversal due to domain nucleation, beginning at the surface due to inhomogeneous local exchange strength between core and surface spins.

Acknowledgment

This work has been supported by Spanish DGICYT of MEC under contract No. MAT2007-01004.

References

[1] Martínez B, Obradors X, Balcells Ll, Rouanet A and Monty C 1998 *Phys. Rev. Lett.* **80** 181
[2] Bonetti E, Del Bianco L, Fiorani D, Rinaldi D, Caciuffo R and Hernando A 1999 *Phys. Rev. Lett.* **83** 2829
[3] Dormann J L, Bessais L and Fiorani D 1998 *J. Phys. C: Solid State Phys.* **21** 2015
[4] Morup S and Tronc E 1994 *Phys. Rev. Lett.* **72** 3278
[5] Nunes W C, Socolovsky L M, Denardin J C, Cebollada F, Brandl A L and Knobel M 2005 *Phys. Rev.* B **72** 212413
[6] Chantrell R W, Walmsley N, Gore J and Maylin M 2000 *Phys. Rev.* B **63** 024410
[7] Morup S, Bodker F, Hendriksen P V and Linderoth S 1995 *Phys. Rev.* B **52** 287
[8] Skumryev V, Stoyanov S, Zhang Y, Hadjipanayis G, Givord D and Nogués J 2003 *Nature* **423** 850
[9] Del Bianco L, Fiorani D, Testa A M, Bonetti E, Savini L and Signoretti S 2002 *Phys. Rev.* B **66** 174418
[10] Koch S A, Palasantzas G, Vystavel T, De Hosson J Th M, Binns C and Louch S 2005 *Phys. Rev.* B **71** 085410
[11] Kim H J, Park J H and Vescovo E 2000 *Phys. Rev.* B **61** 15284
[12] Nogués J, Sort J, Langlais V, Skumryev V, Suriñach S, Muñoz J S and Baró M D 2005 *Phys. Rep.* **422** 65
[13] Nogués J and Schuller I K 1999 *J. Magn. Magn. Mater.* **192** 203
[14] Ceylan A, Baker C C, Hasanain S K and Ismat Shah S 2006 *J. Appl. Phys.* **100** 034301
[15] Sharrock M P and Bodnar R E 1985 *J. Appl. Phys.* **57** 3919
[16] Jiménez-Villacorta F, Huttel Y, Muñoz-Martín A, Ballesteros C, Román E and Prieto C 2007 *J. Appl. Phys.* **101** 113914
[17] Stankiewicz J, Jiménez-Villacorta F and Prieto C 2006 *Phys. Rev.* B **73** 014429
[18] Jiménez-Villacorta F, Muñoz-Martín A and Prieto C 2004 *J. Appl. Phys.* **96** 6224
[19] Jiménez-Villacorta F, Muñoz-Martín A and Prieto C 2006 *Nucl. Instrum. Methods* B **249** 486
[20] Muñoz-Martín A, Prieto C, Ocal C, Martínez J L and Colino J 2001 *Surf. Sci.* **482–485** 1095
[21] Ye Q L, Feng C M, Xu X J, Jin J S, Xia A G and Ye G X 2005 *J. Appl. Phys.* **98** 013906
[22] Kremenovic A, Antic B, Spasojevic V, Vucinic-Vasic M, Jaglicic Z, Pirnat J and Trontelj Z 2005 *J. Phys.: Condens. Matter* **17** 4285
[23] Tung L D, Kolesnichenko V, Caruntu G, Caruntu D, Remond Y, Golub V O, O'Connor C J and Spinu L 2002 *Physica* B **319** 116
[24] Coey J M D 1971 *Phys. Rev. Lett.* **27** 1140
[25] Parker F T, Foster M W, Margulies D T and Berkowitz A E 1993 *Phys. Rev.* B **47** 7885
[26] Pfeiffer H and Schuppel W 1990 *Phys. Status Solidi* a **119** 259
[27] Bean C P and Livingstone J D 1959 *J. Appl. Phys.* **30** 120S
[28] Dormann J L, Fiorani D and Tronc E 1997 *Adv. Chem. Phys.* **98** 283
[29] Denardin J C, Brandl A L, Knobel M, Panissod P, Pakhomov A B, Liu H and Zhang X X 2002 *Phys. Rev.* B **65** 064422
[30] de Witte A M and O'Grady K 1990 *IEEE Trans. Magn.* **26** 1810
[31] Néel L 1949 *Ann. Geophys.* **5** 99
[32] Wohlfarth E P 1979 *Phys. Lett.* A **70** 489
[33] Chantrell W, El-Hilo M and O'Grady K 1991 *IEEE Trans. Magn.* **27** 3570
[34] de Almeida J R L and Thouless D J 1978 *J. Phys. A: Math. Gen.* **11** 983
[35] Wenger L E and Mydosh J A 1984 *Phys. Rev.* B **29** 4156

[36] Victora R H 1989 *Phys. Rev. Lett.* **63** 457
[37] Gittleman J I, Abeles B and Bozowski S 1974 *Phys. Rev.* B **9** 3891
[38] Morup S, Bodker F, Hendriksen P V and Linderoth S 1995 *Phys. Rev.* B **52** 287
[39] Sappey R, Vincent E, Hadacek N, Chaput F, Boilot J P and Zins D 1997 *Phys. Rev.* B **56** 14551
[40] Hickey B J, Howson M A, Greig D and Wiser N 1996 *Phys. Rev.* B **53** 32
[41] Zhang Y D, Budnick J I, Hines W A, Chien C L and Xiao J Q 1998 *Appl. Phys. Lett.* **72** 2053
[42] Stoner E C and Wohlfarth E P 1948 *Phil. Trans. R. Soc.* A **240** 599
[43] Iglesias O, Batlle X and Labarta A 2005 *Phys. Rev.* B **72** 212401
[44] Eftaxias E and Trohidou K N 2005 *Phys. Rev.* B **71** 134406
[45] Fitzsimmons M R, Yashar P, Leighton C, Schuller I K, Nogués J, Majkrzak C F and Dura J A 2000 *Phys. Rev. Lett.* **84** 3986
[46] Nikitenko V I, Gornakov V S, Dedukh L M, Kabanov Y P, Khapikov A F, Shapiro A J, Shull R D, Chaiken A and Michel R P 1998 *Phys. Rev.* B **57** R8111